

contributions

The Characteristics and Design of the Conical Log-Spiral Antenna

JOHN D. DYSON, SENIOR MEMBER, IEEE

Abstract—The balanced conical logarithmic-spiral antenna is considered as a slow-wave locally periodic structure with a slowly varying period. A study of the near fields and their relationship to the far fields has led to the identification of the active region or effective radiating aperture on the antenna and to a clearer understanding of its operating characteristics.

Information of the near- and far-field characteristics and on the input impedance for a wide range of parameters is presented in a form suitable for use in the design of practical antennas.

INTRODUCTION

THE FREQUENCY-INDEPENDENT antennas have found wide application and their general characteristics have been outlined in numerous publications [1], [2]. The purpose of the present paper is to present the characteristics and practical design information for one member of this general class, the balanced two-arm conical logarithmic-spiral antenna, Dyson [3].

Manuscript received March 23, 1964; revised February 25, 1965. This research was sponsored by the Avionics Laboratory, Wright-Patterson AFB, Dayton, Ohio, under Contract AF33(657)-10474.

The author is with the Dept. of Electrical Engineering, University of Illinois, Urbana, Ill.

This study has been guided by the concept, introduced by Mayes, Deschamps, and Patton [4], that the logarithmic-periodic antennas could be considered to be locally periodic structures whose period varies slowly with distance from the point of excitation. It extends this basic concept to the conical log-spiral antenna, by initially comparing the propagation constant measured along the surface of the conical antenna to known propagation constants for the cylindrical bifilar helix.

The study of the propagation constant and other characteristics of the near and far fields of these antennas has led to the identification of the "active region" or effective radiating aperture on the antenna. Successful design of the antenna depends upon knowledge of the position and size of this active region as a function of antenna parameters.

The basic parameters of the conical antenna are defined in Fig. 1. The parameter θ_0 determines the cone angle, and α the rate of wrap of the arms. The angular width of the exponentially expanding arms is defined by the angle δ which is the projection of δ' on a plane perpendicular to the axis of the antenna. These angles

are constant for any given antenna and the radius vector to any point on the arms is given by [3]

$$\rho = \rho_0 \exp b(\phi - \delta) \quad (1)$$

where

$$b = \frac{\sin \theta_0}{\tan \alpha} \quad (2)$$

The edges of the first arm are defined by letting $\delta = 0$, and a fixed value between 0 and π . The second arm is obtained by multiplying the defining equations for the first arm by $e^{-b\pi}$. The orientation of the antenna in the associated spherical coordinate system used for radiation pattern measurements is also indicated.

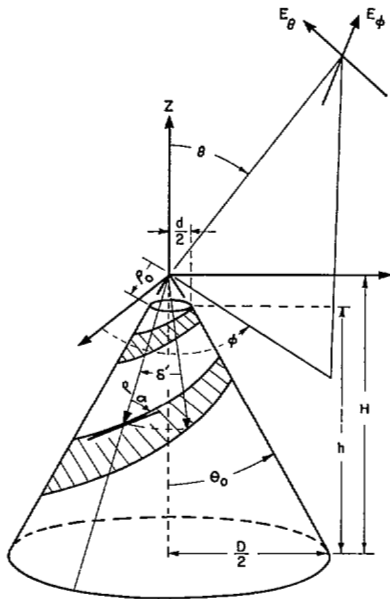


Fig. 1. Conical antenna with associated parameters.

THE ANTENNA AS A LOCALLY PERIODIC STRUCTURE

The parameters involved in a comparison of the conical spiral and cylindrical helical geometries are indicated in Fig. 2, in which is shown one turn or cell of a conical antenna with infinitesimally narrow arms, with l the length of the turn, and a the radius at any point in question. Superimposed upon this is one cell of a cylindrical helix with the same pitch angle, and with a radius equal to the geometric mean radius of the conical cell.

For observations parallel to the axis, the turn-to-turn phasing of the helix is determined to a first approximation by the ratio of the pitch distance p to the turn length l . This assumes a current wave progressing down the arm at the intrinsic phase velocity of the surrounding medium. On the helix this ratio p/l is equal to the sine of the pitch angle or $\cos \alpha$. The ratio of the pitch distance (parallel to the axis) to the turn length on the conical structure is equal to $\cos \alpha \cos \theta_0$.

The ratio (S) of pitch to turn length is also the ratio of the propagation constant k along the arms to the propagation constant β of a wave propagating along the

surface of the cylinder. If we consider the difference between these k/β ratios for the helix and conical spiral, and express this as a function of the helix ratio, we see in Fig. 2 that the difference is simply $1 - \cos \theta_0$. For cones with an included angle of 20° , for example, this difference is approximately $1\frac{1}{2}$ percent. For all conical log-spiral antennas which are good unidirectional radiators, this difference is only a few percent.

This small difference in k/β ratios for the smaller included cone angles would lead one to expect that if we limit our discussion at any one time to a limited portion of the conical antenna there should be, at least for these smaller cones, a close relationship between this portion of the conical structure and some corresponding cylindrical structure.

The variation of the propagation constant on periodic antenna structures can be conveniently displayed on the Brillouin or k/β diagram [5]–[8]. One such diagram for the balanced bifilar helix is shown in Fig. 3. The vertical coordinate is given in units of $ka/\tan \alpha$ which, since $k = 2\pi/\lambda$, is simply the pitch distance in free-space wavelengths. The horizontal scale is the pitch distance expressed in guide wavelengths on the surface of the antenna. For any one helix, since a and α are constant, the only variable involved is the wavelength of operation.

As the frequency of operation is increased the propagation constant increases. If we assume a nondispersive wave along the conductors, we find that there is first a region of slow, closely bound surface waves. As the propagation constant increases still further, there will be strong coupling to a space wave traveling in the opposite direction. The propagation constant becomes complex [9] as the structure radiates with a phasing that provides an end-fire beam directed back toward the point of excitation, i.e., a backfire wave. As the frequency of operation is increased still more, energy is radiated at an angle from the axis of the structure, and then in an end-fire beam in the opposite direction [10].

For the conical antenna there are two variables, the wavelength and the radius a , which vary linearly with distance from the point of excitation. For a fixed wavelength, we see that as a current wave progresses from the point of excitation along a structure with an increasing radius a , the propagation constant might be expected to behave in the manner that we attribute to the cylindrical structure with increasing frequency.

The solution involving the propagation constant along the surface of the cylindrical helix applies to the infinite structure; however, such solutions have been shown to be useful for interpretation of the characteristics of the finite monofilar endfire helix and the finite backfire bifilar helix with thin arms. It is also recognized that extending these concepts to the tapered structure is moving even farther from the basic premise upon which this diagram is based. It is, however, a useful tool in the interpretation of the characteristics of these antennas [11], [12].

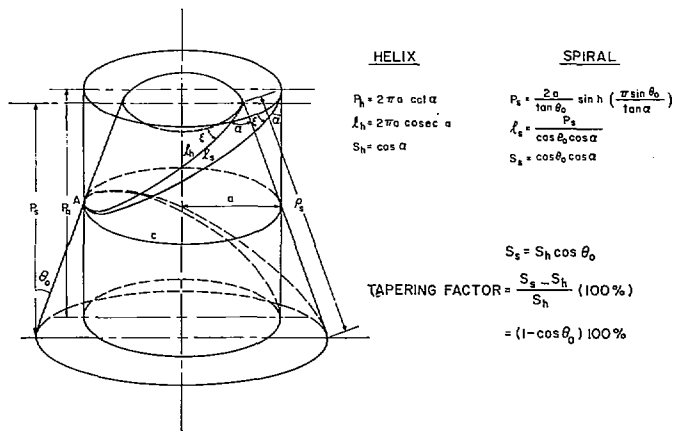


Fig. 2. Corresponding conical spiral and helical cells.

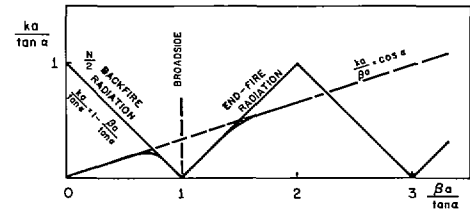
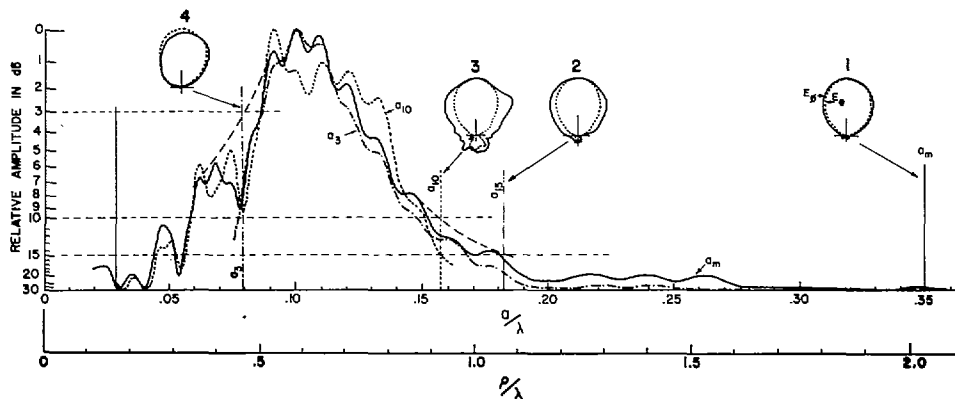


Fig. 3. Brillouin diagram for bifilar helix.

Fig. 4. Amplitude of near fields measured with a small shielded loop probe along the surface of one cone and electric far-field radiation patterns corresponding to a truncation at indicated points ($2\theta_0 = 20^\circ$, $\alpha = 80^\circ$, and $\delta = 90^\circ$).

The curve indicated by a solid line in Fig. 4 is a typical plot of the amplitude of the fields measured by moving a small shielded loop probe parallel to, and 0.03 wavelength from, the surface of one conical antenna. The vertical axis is the relative magnitude of the probed field in decibels, and the horizontal axis is the distance from the apex along the surface of the cone in wavelengths (ρ/λ) and the radius of the cone (a/λ). We observe that there is a region of closely bound waves near the apex of the cone. As the probe is moved along the surface away from the apex, this wave becomes more loosely bound, and more energy is coupled to the probe, until the wave becomes so loosely bound that energy is rapidly lost through radiation, and the amplitude of the near field decays to a negligible value.

As the frequency is changed, this region of rapid decay moves on the antenna so that its location and size in wavelengths remains constant, i.e., the antenna aperture scales with frequency. An arm-to-arm variation in amplitude is visible in the region to the right of the peak amplitude. The standing wave on the apex side of the region of rapid decay appears to be due to an interaction between the wave progressing from the tip down the antenna and the space waves progressing in the opposite direction. When the fields are measured with

the probe very close to the antenna (0.004λ) the amplitude of this first region is only a few dB below the maximum and the amplitude of the standing wave has decreased, e.g., from 10 to 12 dB to less than 1 dB at a radius of 0.05λ . When the probe is moved out to only 0.03 wavelength from the surface of the antenna, the relative amplitude in this region drops by approximately 10 to 15 dB, indicating how tightly the fields are bound to the structure when the cone diameter is small in wavelengths.

THE ACTIVE REGION

Since there appears to be a waveguide region and a radiating region on the antenna, we define the radiating or "active region" to be that region which controls the primary characteristics of the radiated field.

To indicate the extent of the radiating or active region on this antenna, the near-field distribution and radiation patterns are shown in Fig. 4 as the base diameter becomes smaller in wavelengths. The near-field amplitude indicated by the solid curve and the radiation patterns numbered (1) are representative of the antenna without end effect. As successive turns are removed from the base end, there is a negligible change until the antenna is truncated at a radius such that the original

near-field amplitude is approximately 15 dB below the recorded maximum. By the time the base is reduced to this size, a definite change in the half-power beamwidth and the axial ratio is noted. These data and the near-field and far-field data for other antennas, as they were maintained with a fixed size but with a changing frequency of operation, led to the conclusion that the near fields more than 15 dB down from the maximum contributed little to the radiation patterns. The radius of the cone at this point, which we identify as a_{15}^+ , could be considered to be the lower edge of the active region. As the antenna becomes still smaller in wavelengths, the radiation in the direction of the base rapidly increases. The patterns numbered (3), which were recorded for the antenna with a base radius (a_{10}^+), such that the original near-field amplitude was 10 dB below the recorded maximum, are typical of those obtained for a fixed cone size, at a frequency of operation such that the antenna is too small. The effect of these changes in base size, in wavelengths, on the measured field distribution on the small end of the antenna is not great, indicating that we should expect only minor variations in the input impedance.

The effect of a similar truncation of the apex of the cone is shown by the curve labeled a_3 and pattern (4). The vertical solid line indicates the original truncated apex at a radius of approximately 0.03λ . When the antenna is truncated at a radius such that the smoothed level of original field distribution is 3 dB below the maximum, the near-field distribution on the larger turns is perturbed enough to make major modifications in the radiation pattern. This radius we identify as a_3^- . Further truncation produced large changes in the fields and hence in the aperture distribution in the radiating region. In general agreement with these results, calculated radiation patterns based upon the measured near fields of the unperturbed antenna, i.e., without end effect, as the smaller turns were eliminated, showed little change until the antenna was truncated at a point such that the original near-field distribution was approximately 3 dB below the maximum.

Although changes, and in particular a small decrease in beamwidth, may be noted before this limit is reached, these results correlated with the other information led to the adoption of the region from a point 3 dB below the maximum on the apex side (radius a_3^-) to a point 15 dB below the maximum on the base side (radius a_{15}^+) as these fields were measured, as the effective radiating aperture of the antenna in what we could call normal frequency-independent operation. Near-field data recorded under different conditions would necessarily be subject to a different set of limiting values on the active region.

It should be noted that if the line along which the fields are measured were to be rotated around the antenna by 90° , the arms would all be shifted down one-half period and hence the arm-to-arm variations in the field structure would be likewise shifted. The overall

envelope along the peaks of the field in the region of rapid decay would be unchanged. The active region limits were obtained from such a smoothed curve.

Figure 5 is a Brillouin diagram constructed from amplitude and phase data measured on one narrow arm antenna at one frequency of operation. There is indeed a striking resemblance between the variation of the propagation constant with position along the structure and the asymptotic value which we would expect on the bifilar helix with variation of frequency of operation [9]. At the distance from the antenna surface at which these measurements were made, a propagation constant becomes evident by the tenth turn that has a leading phase with increasing distance from the apex. This plot of the variation of the real part of the propagation constant along the surface lies just below the asymptotic line $\cos \alpha \cos \theta_0$. Near turn 18 this propagation constant becomes complex, the real part increases, and the attenuation per cell rapidly increases. From arms 18 to 23 there is more than 25 dB of attenuation. This is the "active region" and the phase center of the radiated field is consistently located in this region, in this case near arm 20. Comparing this figure to Figs. 3 and 4, we note that the majority of this active region and the portion with greatest amplitude near fields is phased for backfire radiation.

When data is recorded at a higher frequency, and the probe separation maintained fixed in wavelengths, the phase variation observed here from turns 11 to 22 is closely repeated at turns 3 through 14. Thus, in contrast to the uniformly periodic structure, the radius at the region of rapid decay (i.e., the active region), expressed in wavelengths, remains essentially fixed on the antenna. If the coupling to the space wave is strong, essentially all of the energy is radiated in the region which is phased for backfire wave radiation and there is a negligible amount left to radiate at any angle from the axis of the structure.

Having defined the active region of the conical antenna in terms of radii of the cone we note how this active region depends upon the antenna parameters. In Fig. 6, the boundaries of this region are plotted as a function of the included cone angle $2\theta_0$ and the spiral angle α . Since both axes of this graph are normalized to the same wavelength these curves give the active region bounds. If, however, the vertical axis is considered to be normalized to the shortest wavelength of operation and the horizontal axis to the longest wavelength of operation, these curves give the required radii of the truncated apex and base of the conical antenna.

A study of the Brillouin diagram in Fig. 5 indicates that the active region of the $\alpha = 60^\circ$ antenna, for example, should be closer to the apex of the cone than for the $\alpha = 80^\circ$ antenna. Figure 6 shows that the onset of radiation does occur at a smaller radius, but the loose spirals are less efficient radiators; the net effect is that these antennas radiate over a considerably wider region on the antenna. The result is an active region that starts

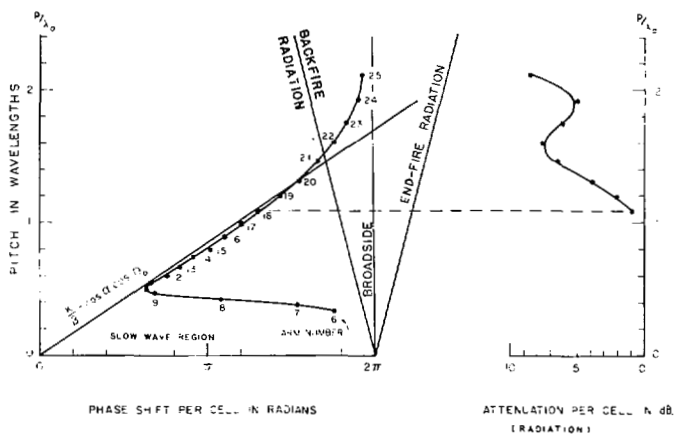


Fig. 5. Measured Brillouin diagram for one conical spiral antenna.

at a smaller radius and, particularly for $2\theta_0 > 10^\circ$, extends to a larger radius than the equivalent region on the antennas with tighter spirals.

These limits on the active region were based upon near-field measurements. In terms of the far-field patterns, they are most accurate for cones with total included angles of approximately 20° . They tend to become more conservative as the cone angle decreases and slightly optimistic for greater cone angles.

If the active region had no width, the operating bandwidth of the antenna would be given by the ratio of the radius of the base to the radius of the truncated apex. Following the convention proposed by Carrel [13] for the log-periodic dipole arrays, this ratio is defined to be the bandwidth of the structure B_s .

$$B_s = \frac{D}{d}$$

It is apparent that the operating bandwidth of the antenna is always less than the bandwidth of the structure by a factor defined to be the bandwidth of the active region B_{ar}

$$B_{ar} = \frac{a_{15}^+}{a_3^-}$$

Hence, the antenna operating bandwidth B is given by

$$B = B_s / B_{ar}$$

Figure 6 includes a grid indicating the active region bandwidth B_{ar} as a function of antenna parameters.

For many applications, considerable pattern distortion can be tolerated at the ends of the operating bandwidth; hence, the antenna can be operated to a smaller size. For such applications Fig. 7 gives the active region bounds as radii a_3^- and a_{10}^+ , where a_{10}^+ is the radius at which the unperturbed near-field amplitude is 10 dB below the recorded maximum, and patterns number (3) in Fig. 4 are typical at the lowest frequencies of operation. At these frequencies the typical axial ratio on axis should be 4.7 dB or less. For operation only to the bounds shown in Fig. 6, the axial ratio on axis should be approximately 3 dB or less at the lowest frequencies.

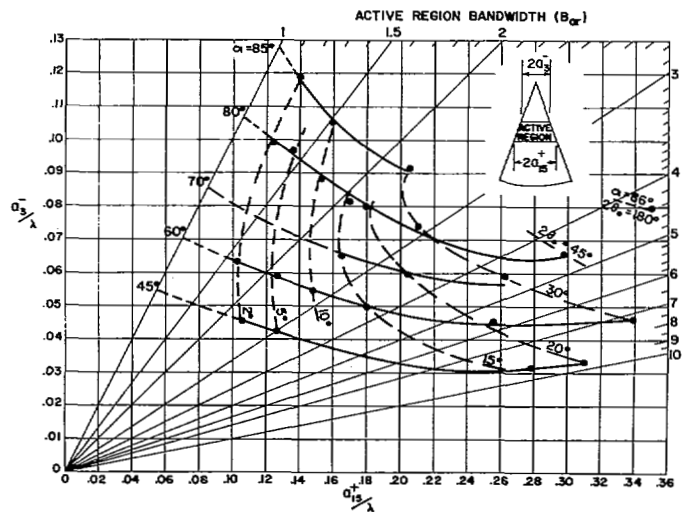


Fig. 6. Bounds of the active region in terms of the radius of the cone. Data for the self-complementary antenna ($\delta = 90^\circ$).

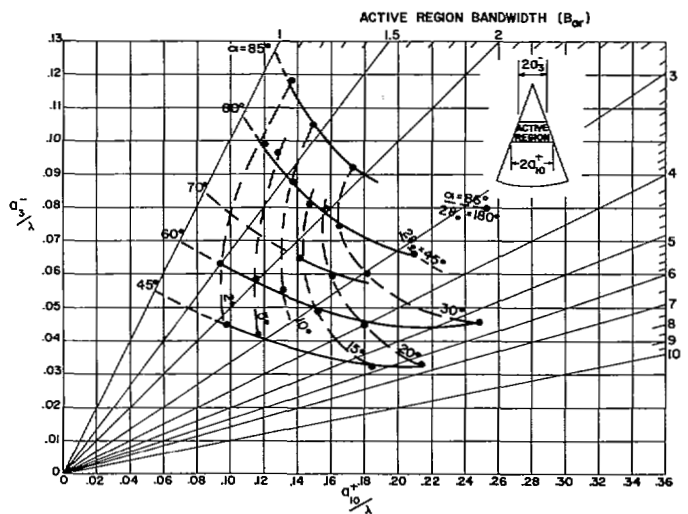


Fig. 7. Bounds of the active region that may be used for design if appreciable pattern distortion is permissible at lowest operating frequency ($\delta = 90^\circ$).

CHARACTERISTICS OF THE RADIATION FIELDS

In Fig. 8 typical electric field radiation patterns are shown as a function of the included cone angle, and the spiral angle α . The well-formed relatively narrow beam for small cone angles with $\alpha = 80^\circ$ is indicative of essentially all turns of the active region being phased for backfire radiation. As the active region broadens, the radiation pattern broadens and exhibits a tendency to show a multiple beam effect with corresponding irregularities or "ears." It is worth noting that this relationship between aperture size and antenna directivity is exactly opposite to the usual case. It is brought about because the phase distribution across the effective radiating aperture is such that all parts of the aperture are phased to radiate in progressively different directions.

Increased directivity is obtained for the periodic structure by extending the radiating aperture over more elements. In principle, this concept is applicable to the tapered periodic structures and may be realizable

for a slight taper. As the taper is increased to obtain a practical size antenna that will scale over a wide range of frequencies, it is no longer possible to maintain the required phasing for backfire radiation over a large aperture. The larger turns, or more widely spaced elements, are phased to radiate energy at an angle from the axis of the antenna. Hence, for any given cone angle, the net effect is an inversion of the usual aperture size-directivity relationship.

This effect is shown in Fig. 9 where the relative magnitude and phase of the tangential magnetic field measured along the surface of three log-spiral antennas, each with an included cone angle of 15° , is shown. When the arms are wound fairly tightly, $\alpha = 80^\circ$, the leading phase over a relatively narrow aperture concentrates the radiated energy in the backward direction. As the rate of spiral is relaxed the relative radiating efficiency of the aperture decreases, and hence the aperture size increases. The slope of the phase curve is decreased and the last few turns in the active region radiate appreciable energy at an angle from the axis of the cone. When the angle of wrap α is decreased to 45° , a major portion of the active region is phased for broadside radiation. To maintain good backfire patterns the leading edge of the effective aperture must have an excess of phase shift for backfire radiation, and this aperture must be an efficient radiator.

If we recall from Figs. 3 and 5 that the ratio of the velocity of propagation of the surface wave to a free-space wave was approximately $\cos \alpha \cos \theta_0$, and solve for the intersection of this asymptotic line and the region boundary given by

$$\frac{ka}{\tan \alpha} = 1 - \frac{\beta a}{\tan \alpha}$$

we obtain the expression

$$\frac{a}{\lambda} = \frac{1}{2} \frac{\sin \alpha \cos \theta_0}{1 + \cos \alpha \cos \theta_0}.$$

This and similar expressions for the intersection of the asymptote and the lines $\beta a = \tan \alpha$ (broadside radiation) and

$$\frac{\beta a}{\tan \alpha} = 1 + \frac{ka}{\tan \alpha}$$

(end-fire radiation) have been plotted as the dashed curves in Fig. 10.

The radii a_3^- and a_{15}^+ that outline the active region have also been plotted for 2° and 20° cones. Although this is only an approximate indication of the relative phasing of the radiating aperture, it clearly indicates the phenomena observed in Fig. 9. Recalling the amplitude distribution from Figs. 4 and 9, we see that for the 20° cones the major part of the radiating aperture of the tightly wrapped antennas is phased for backfire radiation. From these we get relatively narrow well-formed beams. However, as the angle α decreases, the net result of the radiation from the wider active region is a

wide beam. The backfire phasing of the 2° cones, for α greater than 70° , is clearly evident.

The approximate half-power beamwidths of the radiated fields of the conical antennas are plotted in Fig. 11. The patterns recorded by orthogonally oriented receiving antennas E_θ and E_ϕ differ typically 8° to 10° in beamwidth. The values given in Fig. 11 are the average of these beamwidths. In addition, this mean level of the beamwidth must be evaluated in conjunction with the indicated variation in beamwidth around this level shown in Fig. 12. This indicated variation in beamwidth is caused by the fact that the radiated beam, which may not be rotationally symmetric, rotates about the axis of the antenna as the frequency of operation is changed [14]. This effect, and the fact that the practically constructed antenna will not scale exactly at all frequencies, causes a variation in beamwidth in a fixed plane of observation as the antenna is operated over a very wide range of frequencies. This variation can be minimized for operation over a reduced bandwidth and would be on the order of that for any conventional antenna when operated over the bandwidths of a few percent for which such antennas are designed.

The approximate directivity with respect to a circularly polarized isotropic source plotted in Fig. 11 was obtained from the use of these average half-power beamwidths in the expression [15]

$$D = 10 \log_{10} \frac{32\,600}{\phi_1 \theta_1} \text{ dB},$$

where ϕ_1 and θ_1 are the average half-power beamwidths in two orthogonal planes.

The front-to-back ratios of the radiated fields are plotted in Fig. 13. This is the typical minimum value that should be expected for a well-constructed antenna operated at a frequency such that there is no effect due to the truncated base or tip. The decrease in front-to-back ratio with increasing cone angle is to be expected since the planar structure is bidirectional.

The antenna is elliptically, and essentially circularly, polarized in any direction in which there is substantial radiation. Typical values of axial ratio recorded at angles from the axis of a 20° antenna are shown in Fig. 14. The lower curve is indicative of the increased beamwidth and increased energy radiated in directions approaching that perpendicular to the axis of the antenna as the rate of wrap α is decreased.

The conical log-spiral antennas do not have a unique center of phase, however over a portion of the main beam an "apparent phase center" may be defined [16]. As shown in Fig. 15, the apparent phase centers of the smaller cone antennas lie well below the slow-wave region boundary on the Brillouin diagram. For $2\theta_0 \leq 20^\circ$ the position of the apparent phase center can be given by the straight-line approximation in Fig. 15. In terms of the cone radius this may be expressed as:

$$a/\lambda = \frac{1}{2\pi} \frac{1.2 \sin \alpha}{1.4 + \cos \alpha}.$$

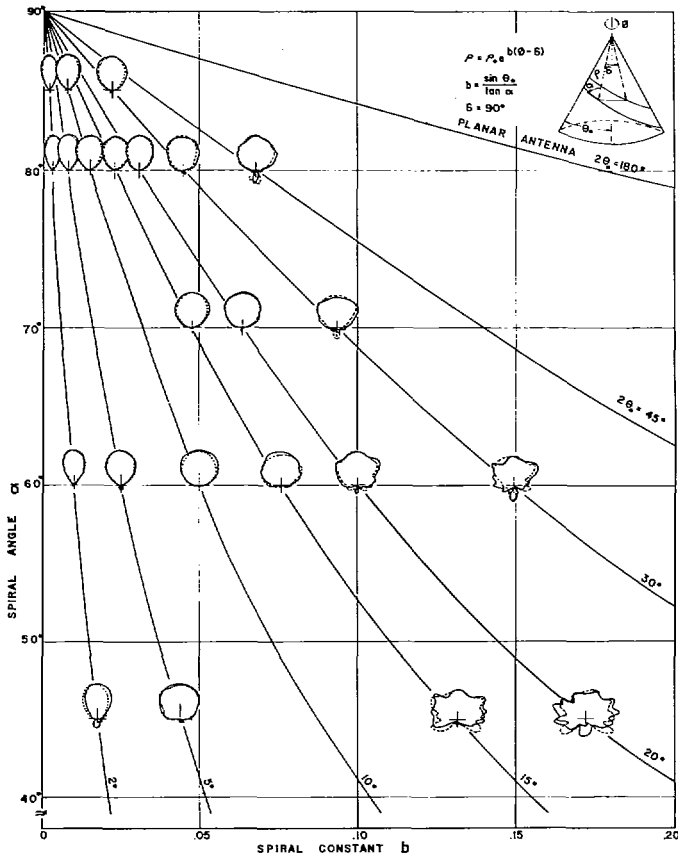


Fig. 8. Typical electric field radiation patterns shown for two orthogonal field polarizations ($\delta = 90^\circ$).

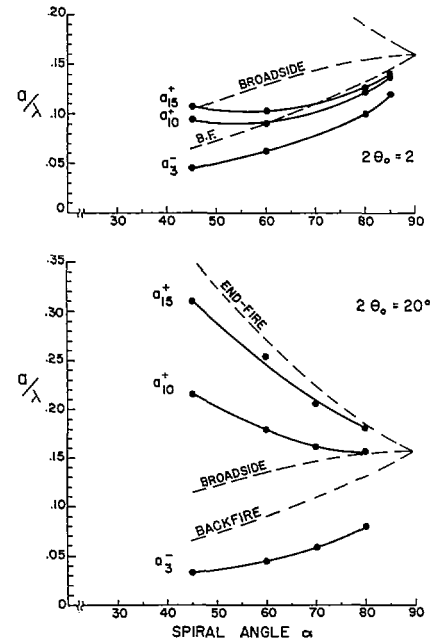


Fig. 10. Approximate turn-to-turn phase variation over the active region ($\delta = 90^\circ$).

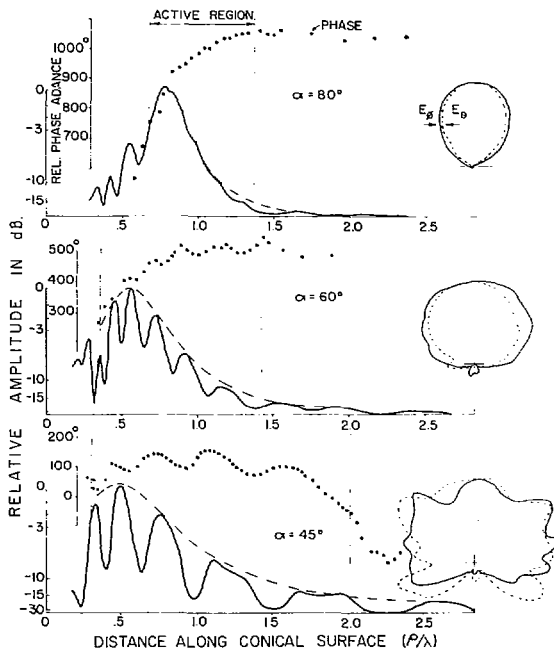


Fig. 9. Relative amplitude and phase of magnetic fields measured along the surface of conical antennas ($2\theta_0 = 15$, $\delta = 90^\circ$), and corresponding far-field radiation patterns.

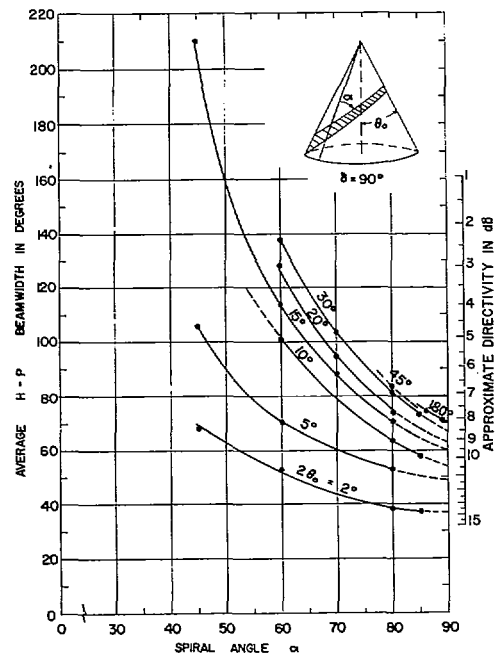


Fig. 11. Average half-power beamwidth and approximate directivity of the conical log-spiral antennas ($\delta = 90^\circ$).

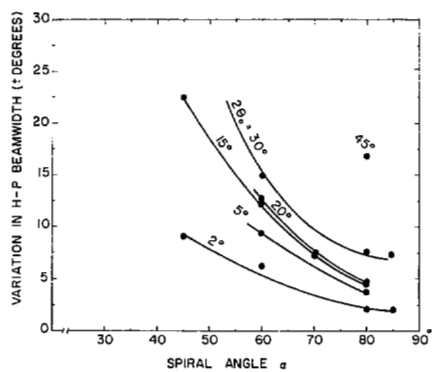


Fig. 12. Approximate variation in half-power beamwidth to be expected when antenna is operated over wide bandwidths.

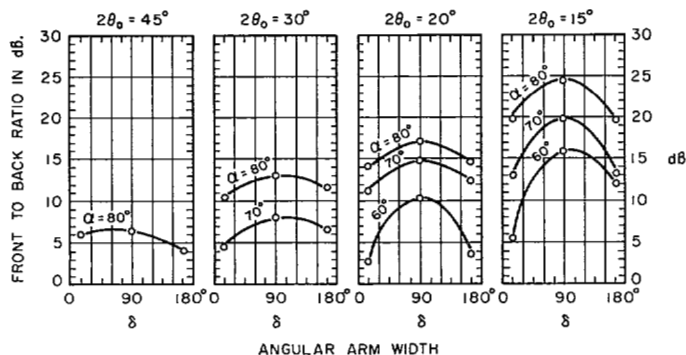


Fig. 13. Minimum front-to-back ratio of radiation patterns as a function of θ_0 , α , and δ .

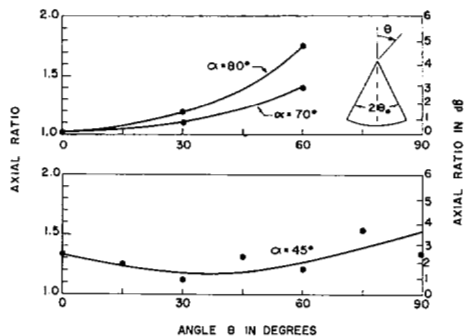


Fig. 14. Typical variation of axial ratio off the axis of antenna. Measured for one antenna with $2\theta_0 = 20^\circ$, $\delta = 90^\circ$.

The heavy weighting of the portion of the aperture nearest the apex of the cone, due to the high amplitude fields present there, tends to keep the phase center in this general region even though the radiation region, albeit at lower amplitudes, extends considerably farther down the antenna.

THE ANTENNA FEED SYSTEM

The two-arm conical antenna is a symmetrical structure, and when excited in a balanced manner it radiates a beam on the axis of the cone without squint or tilt. In all cases a tilt in the radiation pattern can be traced to the physical construction or to imbalance in the feed.

The antenna may be excited by bringing a balanced transmission line along the axis, to the apex of the cone, and connecting one wire to each arm. It is preferable, although not necessary, that this be a shielded line. The presence of a metallic shield or cylinder *on axis* has a minimum of effect on the antenna characteristics if the diameter of this cylinder (or metal cone) is no more than one third the diameter of the antenna at any point on the axis.

The transition from an unbalanced coaxial line to a balanced line may be made by placing a balun inside the antenna if the balun is nonradiating and not affected by the fields inside the cone. Conventional baluns may fall into this class, but are very limited in bandwidth. The tapered line balun [17] with its extremely wide bandwidth would seem to be ideally suited for use with this antenna. When placed inside the antenna, however, there appears to be an interaction or interference between the fields around the balun and those of the antenna, with the result that a truly balanced feed is seldom realized. For some purposes, however, the degradation of the pattern due to the use of this balun can be tolerated.

The excellent coaxial hybrids now on the market make satisfactory baluns [18]. These units provide equal amplitude out-of-phase signals at the side arms. Fifty-ohm coaxial cables connected to these arms may be carried along the axis of the cone, and the two center conductors of the cables thus become a shielded balanced 100-ohm transmission line. For maximum symmetry, and to prevent the two outer sheaths from becoming a transmission line for any unbalanced currents, these cables should be bonded together or placed inside a metal tube or cylinder. Most of these hybrids are limited to an octave bandwidth and provision must be made for replacing or switching of hybrids. In the VHF and UHF range, however, low-power hybrids have recently become available for use over ten-to-one and greater bandwidths.

To overcome the limiting bandwidths of the baluns, the method of feeding the antenna by carrying the coaxial cable along one arm was devised [14]. To maintain physical symmetry a similar cable must be placed on the other arm. This method, which has been termed the "infinite balun" feed, remains the most satisfactory

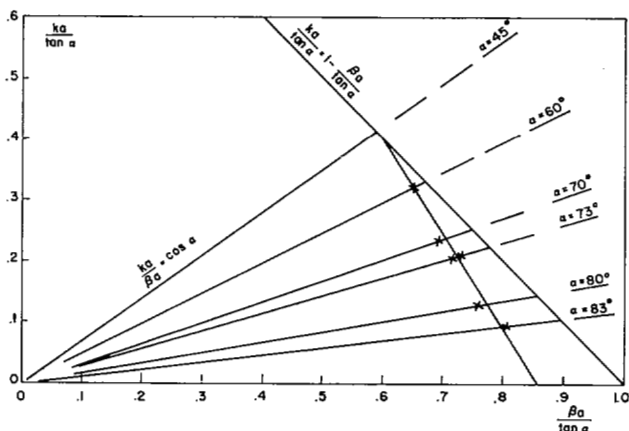


Fig. 15. Measured "apparent phase centers" for several conical antennas ($2\theta_0 = 20^\circ$).

method if the physical presence of the cable does not limit the size of the truncated apex region, and if the loss in the relatively long length of cable can be tolerated. It is a truly balanced feed under the condition that the antenna currents have decayed to a negligible value at the truncated base of the cone and a symmetrical connection is maintained at the feed point.

INPUT IMPEDANCE OF THE ANTENNA

The geometry of the truncated tip, including the possible presence of the feed cable on the antenna arms, has a marked effect upon the character of the input impedance of the antenna. Since there is an unlimited combination of cable diameter-truncated tip combinations, it appears to be meaningful to present only the impedance of the basic antenna when fed on axis, and indicate the trend as you depart from this basic structure.

Figure 16 indicates the effect that the feed geometry can exert on the measured impedance. Symmetry, balance, and tapered leads from the axis to the surface of the cone are required.

The use of the coaxial hybrids as baluns makes possible a very convenient method of making balanced impedance measurements, if identical slotted lines are inserted in the coaxial lines between the antenna and the hybrid [19].

To determine the impedance level of the antennas, measurements referred to a reference plane at the tips of the tapered leads on the truncated apex of the cone were made over a five-to-one bandwidth. The normalized impedances plotted on the Smith Chart were enclosed by a circle. The "center" of this circle, chosen to make the hyperbolic distance to all parts of the circle a constant [20], was considered to be the characteristic impedance of the antenna. The maximum VSWR referred to this characteristic impedance was typically 1.3 to 1.4 to 1.

The variation of the characteristic impedance with arm width is shown in Fig. 17. The input impedance of the antenna is primarily controlled by the arm width, varying from around 320 ohms, for the very narrow arm antennas, to around 80 ohms, for the corresponding very wide arm antennas. The impedance increases as the included cone angle increases, with that for the self-complementary antennas ($\delta=90^\circ$) approaching the theoretically predicted 60π or 189 ohms for the planar antenna [21]. The measured impedance variation with change in the spiral angle α was small, although a tendency for this impedance to increase with increasing α was observed.

The apparently clear trend in impedance level with cone angle shown in Fig. 17 was not observed for all angles, and the impedance levels for cone angles less than 15° were not lower than those shown for 15° . For example, for $2\theta_0=5^\circ$, $\alpha=80^\circ$, the characteristic impedance measured for $\delta=16, 90$, and 164° was approximately 300, 185, and 72 ohms, respectively. The imped-

ance levels of these antennas have not yet been precisely defined. Figure 17 does indicate approximate levels for design and the trend in this level with angular arm width.

The presence of cable on the arms tends to give the narrow arms near the apex an effectively greater cross section and, hence, shifts the impedance level. An approximate curve of the measured input impedance for an antenna with $2\theta_0=20^\circ$, $\alpha=60$, and a tip truncated at

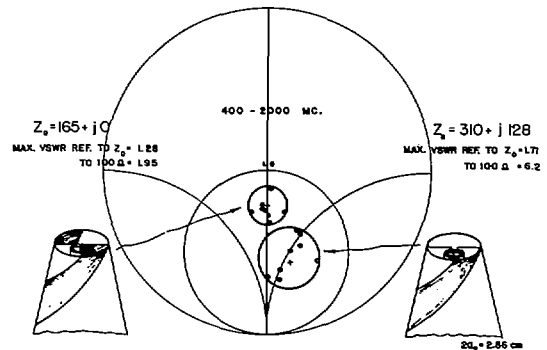


Fig. 16. Effect of the feed region geometry on the input impedance.

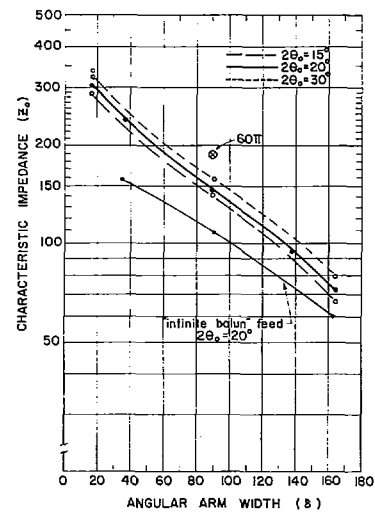


Fig. 17. Approximate characteristic impedance level of the conical log-spiral antenna as a function of the angular arm width.

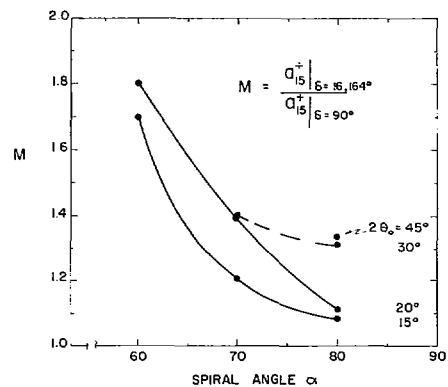


Fig. 18. Approximate ratio of the radius at the base end of the active region for very narrow or very wide arm widths to that for the self-complementary antenna.

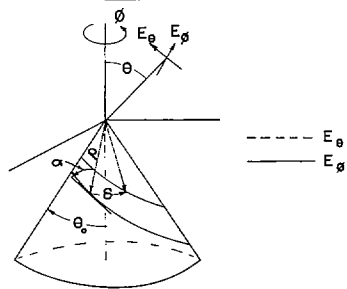


Fig. 19. Typical electric field radiation patterns indicating general change in shape with cone angle θ_0 , spiral angle α , and angular arm width δ .

0.75 inch, fed with RG141/U cable of diameter 0.141 inch is shown. This curve indicates the general impedance level for this particular cable-truncation combination only. The maximum VSWR referred to this impedance level was approximately 1.75 to 1. The tapered leads at the truncation are still required if the width of the arm on the surface of the cone at this truncation is substantially wider than the diameter of the cable.

The impedance bandwidth is consistently greater than the radiation pattern bandwidth and hence the active region was defined in terms of the latter.

EFFECT OF ARM WIDTH

The angular width of the expanding antenna arms is defined in terms of δ where $0 < \delta < \pi$.

In nearly all cases, the characteristics of these antennas have been investigated for very narrow arm structures ($\delta = 16^\circ$), for very wide arm structures ($\delta = 164^\circ$), and for $\delta = 90^\circ$. This latter structure is defined to be self-complementary in the sense that the geometry of the arms and the space between arms is identical except for a rotation of 90° about the axis of the structure.

With the exception of the impedance which is directly related to the arm width, nearly all data presented thus far have been for the self-complementary antenna. Changes in the other characteristics do occur as this width is changed. For example, the rate of decay of the near fields becomes less as δ departs from 90° . Thus a_{15}^+ becomes larger. In Fig. 18 a factor M indicating the ratio of the maximum radius required for very narrow or very wide arms to that required for arms with $\delta = 90^\circ$ has been plotted. For values of δ between 90° and 16° or 164° linear interpolation from $M = 1.0$ to the indicated value should be sufficient. Since a_3^- changes little compared to the change in a_{15}^+ , this modification factor M can also be taken to be the ratio of the active region bandwidths B_{ar} , for $\delta = 16^\circ$ and 164° , to that for $\delta = 90^\circ$.

For $2\theta_0 \leq 20^\circ$ the variation with δ is less for $\alpha \geq 75^\circ$, and hence, for these small-cone fairly tightly wrapped antennas it is possible to use thin arms and the constant width wire or cable arms version of the antenna [3], with only a small change in characteristics of the radiation pattern. The change in the electric field radiation patterns with change in arm width is indicated in Fig. 19. The principal change is an increase in beamwidth (5° to 8° for $\alpha = 80^\circ$) brought about by the increase in active region width.

These patterns are typical of those to be expected when the antenna is operated at frequencies such that there is no distortion due to the truncation of the base or tip. As the frequency of operation is decreased and the lower edge of the active region becomes distorted by the truncated base, the amplitude of the back lobe will increase rather rapidly. As the leading edge of the active region moves to the truncated tip, the pattern beamwidth may at first become narrower and the pattern become rough. Any lack of precision in construction at the apex region will cause pattern tilt or distortion. A further

increase in frequency may cause the pattern to broaden with a tendency to break into lobes.

Radiation patterns for the very loosely wrapped antennas, $\alpha = 45^\circ$, with self-complementary width arms only are shown. As the arm width deviates from $\delta = 90^\circ$ for antennas with $2\theta_0 \geq 15^\circ$ and $\alpha \leq 45^\circ$, the pattern breaks into many lobes with a major portion of the energy radiated in the direction of the base.

A decrease in the front-to-back ratio of the radiation patterns, as indicated in Fig. 13, may be noted as δ departs from 90° .

ANTENNA DESIGN AND CONSTRUCTION

The antenna engineer is usually interested in designing an antenna which has a given directivity or radiation pattern beamwidth and input impedance over a given frequency band. A satisfactory design should be obtained from the previously plotted data. The data was obtained for antennas constructed of 2-mil thick copper, etched on 10-mil teflon-impregnated fiber glass, with a balanced two-coaxial line feed carried along the axis of the cone. Hence, the data should be representative of the basic antenna structure. The use of an infinite balun feed or a cable approximation to the expanding arms should modify the antenna characteristics in a predictable manner, since the cable gives an effectively greater width to narrow arms.

Half-power beamwidths on the order of 40° to 50° can be obtained with the small cone antennas. However, when very wide bandwidths are to be covered these antennas may become quite long. Physical requirements, such as allowable length or height, may dictate the choice of the wider cone angles and a compromise of antenna characteristics. The antenna length or height in terms of the longest wavelength of operation λ_L may be expressed as

$$\frac{h}{\lambda_L} = \frac{1}{2 \tan \theta_0} \left[\frac{D}{\lambda_L} - \frac{1}{B} \frac{d}{\lambda_N} \right].$$

In constructing these antennas it must be realized that they are potentially extremely wide-band antennas, and are expected to perform with constant characteristics over these bandwidths. To do this, the active region must be able to scale to a constant geometry and to constant physical parameters expressed in wavelengths at all frequencies. Hence, *all* such parameters should scale in size with distance from the apex. Symmetry, balance, and detail and precision of construction are important. Violation of any of these principles can only lead to degradation of the antenna characteristics as the frequency of operation is varied.

CONCLUSIONS

The conical log-spiral antenna can be considered to be a locally periodic structure, with slowly varying period. A study of the antenna in this context has led to ready identification of many of its characteristics.

This study indicates that the fairly tightly spiraled self-complementary antenna tends to be the "optimum antenna," in the sense that it has the narrowest active region and, hence, the greatest operating bandwidth for a given physical size, and the most compact symmetrical radiated beam with the least energy radiated in back lobes. The input impedance, however, depends primarily upon arm width, with typical values of 140 to 165 ohms for these self-complementary structures.

ACKNOWLEDGMENT

The author gratefully acknowledges the assistance of A. L. Davidson, G. R. Fruehling, M. D. Johnson, V. P. Rash, R. J. Kopczyk, and other members of the University of Illinois Antenna Laboratory, who helped with the measurement program carried on during this investigation.

REFERENCES

- [1] Dyson, J. D., Frequency-independent antennas—survey of development, *Electronics*, vol 35, Apr 20, 1962, pp 39-44 (includes extensive list of early references).
- [2] Jordan, E. C., G. A. Deschamps, J. D. Dyson, and P. E. Mayes, Developments in broadband antennas, *IEEE Spectrum*, vol 1, Apr 1964, pp 58-71.
- [3] Dyson, J. D., The unidirectional equiangular spiral antenna, *IRE Trans. on Antennas and Propagation*, vol AP-7, Oct 1959, pp 329-334.
- [4] Mayes, P. E., G. A. Deschamps, and W. T. Patton, Backward-wave radiation from periodic structures and application to the design of frequency-independent antennas, *Proc. IRE (Correspondence)*, vol 49, May 1961, pp 962-963.
- [5] Oliner, A. A., Leaky waves in electromagnetic phenomena, in *Electromagnetic Theory and Antennas*, E. C. Jordan, Ed. New York: Pergamon, 1963, pp 837-856.
- [6] Rumsey, V. H., Propagation over a sheet of sinusoidal wires and its application to frequency independent antennas, *ibid.*, pp 1011-1030.
- [7] Mittra, R., and K. E. Jones, Theoretical Brillouin ($k-\beta$) diagram for monopole and dipole arrays and their application to log-periodic antennas, *1963 IEEE Internat'l Conv. Rec.*, pt 1, pp 118-128.
- [8] Hudock, E., and P. E. Mayes, Propagation along periodic monopole arrays, *1963 G-AP Internat'l Symp. Digest*, pp 127-132.
- [9] Klock, P. W., and R. Mittra, On the solution of the Brillouin ($k-\beta$) diagram of the helix and its application to helical antennas, *1963 G-AP Internat'l Symp. Digest*, pp 99-103.
- [10] Ishimaru, A., and H. S. Tuan, Theory of frequency scanning of antennas, *IRE Trans. on Antennas and Propagation*, vol AP-10, Mar 1962, pp 144-150.
- [11] Dyson, J. D., The coupling and mutual impedance between conical log-spiral antennas in simple arrays, *1962 IRE Internat'l Conv. Rec.*, pt 1, pp 165-182.
- [12] Dyson, J. D., and G. L. Duff, Near field measurements on the conical log-spiral antenna, *1963 G-AP Internat'l Symp. Digest*, pp 137-142.
- [13] Carrel, R., The design of log-periodic dipole antennas, *1961 IRE Internat'l Conv. Rec.*, pt 1, pp 61-75.
- [14] Dyson, J. D., The equiangular spiral antenna, *IRE Trans. on Antennas and Propagation*, vol AP-7, Apr 1959, pp 181-187.
- [15] Stegen, R. J., The gain-beamwidth product of an antenna, *IEEE Trans. on Antennas and Propagation (Correspondence)*, vol AP-12, Jul 1964, pp 505-506.
- [16] Dyson, J. D., and R. E. Griswold, Measurement of the phase centers of antennas, Tech Rept 66, Antenna Lab., University of Illinois, Urbana, Dec 1963.
- [17] Duncan, J. W., and V. P. Minerva, 100:1 bandwidth balun transformer, *Proc. IRE*, vol 48, Feb 1960, pp 156-164.
- [18] Alford, A., and C. B. Watts, Jr., A wide band coaxial hybrid, *1956 IRE Conv. Rec.*, pt 1, pp 171-179.
- [19] Dyson, J. D., Balanced impedance measurements with a coaxial system, Tech Rept, Antenna Lab., University of Illinois, Urbana, to be published.
- [20] Deschamps, G. A., A hyperbolic protractor, Federal Telecommunication Labs., Nutley, N. J.; 1953.
- [21] Rumsey, V. H., Frequency independent antennas, *1957 IRE Nat'l Conv. Rec.*, pt 1, pp 114-118.

Antenna and Wave Theories of Infinite Yagi-Uda Arrays

R. J. MAILLOUX, SENIOR MEMBER, IEEE

Abstract—An integral equation for the propagation constant along an infinitely long Yagi structure is derived by expanding the vector potential function for such an array in terms of the spatial harmonic solutions of wave theory. This equation is shown to be identical with the integral equation derived on the basis of array theory and transformed by the Poisson summation formula.

With the identity of array theory and this new wave theory formation established, the wave theory is used to discuss allowed

wave solutions and the physical characteristics required of dipoles in order that they support a wave solution.

The fundamental integral equation is solved by means of the array theory of King and Sandler; the numerical results are found to agree quite well with previously published data.

Finally, the problem of two parallel nonstaggered Yagi arrays is considered, and it is shown that the propagation constant of the composite structure either decreases or increases over that of the isolated array depending upon whether the symmetric or the anti-symmetric mode is excited. Some peculiar effects are noted with respect to this antisymmetric solution, and these lead to the existence of conditions under which no unattenuated wave solution is possible. This is referred to as the "cutoff condition."

Numerical results are achieved which agree very well with experimental data obtained as part of this research.

Manuscript received September 14, 1964; revised March 4, 1965. The research in this paper was supported in part by National Science Foundation Grant GP851 and in part by Joint Services Contract Nonr 1866(32).

The author is with the Gordon McKay Laboratory of Applied Science, Harvard University, Cambridge, Mass.